

Preparation and cooling performance analysis of double-layer radiative cooling hybrid coatings with $TiO_2/SiO_2/Si_3N_4$ micron particles

Yang-Chun Zhao(赵洋春) and Yong-Min Zhou(周勇敏)
Citation: Chin. Phys. B, 2023, 32 (**11**): 114401. DOI: 10.1088/1674-1056/acdac0
Journal homepage: http://cpb.iphy.ac.cn; http://iopscience.iop.org/cpb

What follows is a list of articles you may be interested in

Infrared cooling properties of cordierite

Si-Heng Chen(陈思衡), Xiao-Xiong Wang(王晓雄), Guang-Di Nie(乜广弟), Qi Liu(刘奇), Jin-Xia Sui(隋金霞), Chao Song(宋超), Jian-Wei Zhu(朱建伟), Jie Fu(付洁), Jun-Cheng Zhang(张君诚), Xu Yan(闫旭), Yun-Ze Long(龙云泽)
Chin. Phys. B, 2019, 28 (**6**): 064401. DOI: 10.1088/1674-1056/28/6/064401

pectral enhancement of thermal radiation by laser fabricating grating structure on nickel surface

Liu Song (刘嵩), Liu Shi-Bing (刘世炳)
Chin. Phys. B, 2015, 24 (**5**): 054401. DOI: 10.1088/1674-1056/24/5/054401

Near-field radiative heat transfer in mesoporous alumina

Li Jing (李静), Feng Yan-Hui (冯妍卉), Zhang Xin-Xin (张欣欣), Huang Cong-Liang (黄丛亮), Wang Ge (王戈)
Chin. Phys. B, 2015, 24 (**1**): 014401. DOI: 10.1088/1674-1056/24/1/014401

A comparison of different entransy flow definitions and entropy generation in thermal radiation optimization

Zhou Bing (周兵), Cheng Xue-Tao (程雪涛), Liang Xin-Gang (梁新刚)
Chin. Phys. B, 2013, 22 (**8**): 084401. DOI: 10.1088/1674-1056/22/8/084401

Thermal conductivity of a kind of mesoporous silica SBA-15

Huang Cong-Liang (黄丛亮), Feng Yan-Hui (冯妍卉), Zhang Xin-Xin (张欣欣), Li Jing (李静), Wang Ge (王戈)
Chin. Phys. B, 2013, 22 (**6**): 064401. DOI: 10.1088/1674-1056/22/6/064401

Preparation and cooling performance analysis of double-layer radiative cooling hybrid coatings with $TiO_2/SiO_2/Si_3N_4$ micron particles

Yang-Chun Zhao(赵洋春) and Yong-Min Zhou(周勇敏)†

College of Materials Science and Engineering, Nanjing Tech University, Nanjing 211816, *China*

(Received 3 March 2023; revised manuscript received 18 May 2023; accepted manuscript online 2 June 2023)

Passive daytime radiative cooling is achieved by radiating heat into outer space through electromagnetic waves without energy consumption. A scalable double-layer coating with a mixture of TiO_2, SiO_2, and Si_3N_4 micron particles for radiative cooling is proposed in this study. The finite-difference time-domain algorithm is used to analyze the influence of particle size and coating thickness on radiative cooling performance. The results of the simulation show that the particle size of 3 μm can give the best cooling performance, and the coating thickness should be above 25 μm for SiO_2 coating. Meanwhile, the mixture of SiO_2 and Si_3N_4 significantly improves the overall emissivity. Through sample preparation and characterization, the mixture coating with a 1:1 ratio addition on an Al substrate exhibits high reflectivity with a value of 87.6% in the solar spectrum, and an average emissivity of 92% in the infrared region (2.5 μm–15 μm), which can be attributed to the synergy among the optical properties of the material. Both coatings can theoretically be cooled by about 8 °C during the day and about 21 °C at nighttime with $h_c = 4\ \mathrm{W{\cdot}m^{-2}{\cdot}K^{-1}}$. Furthermore, even considering the significant conduction and convection exchanges, the cooling effect persists. Outdoor experimental results show that the temperature of the double-layer radiative cooling coating is always lower than the ambient temperature under direct sunlight during the day, and can be cooled by about 5 °C on average, while lower than the temperature of the aluminum film by almost 12 °C.

Keywords: radiative cooling, coatings, thermal radiation, infrared emissivity

PACS: 44.40.+a, 42.79.Wc, 03.65.Nk **DOI:** 10.1088/1674-1056/acdac0

1. Introduction

Radiative cooling can create cooling effect without energy input, and it has been rapidly developed as a passive cooling method to alleviate the energy crisis and environmental pollution. It operates in a wavelength range from 8 μm to 13 μm (also known as the "sky window" or "atmospheric window"),[1,2] because the atmosphere around the earth is transparent to visible light, while thermal energy from surface objects is emitted into outer space in the form of infrared radiation, which is opaque to most wavelengths of infrared radiation.[3,4]

In the past decades, the radiative cooling has been studied. Its potential application for nighttime cooling has been practically demonstrated.[5–8] Materials must have good infrared (IR) emission within the atmospheric window to achieve radiative cooling at night. An SiO film covered by Granqvist forms a composite structure on an Al substrate.[6] They demonstrated a strong absorption resonance at the 10 μm based on SiO intrinsic phonon resonance, thereby realizing infrared emission. In addition to solid materials, some selective infrared emitting gases, such as ammonia (NH_3), ethylene (C_2H_2), and ethylene oxide (C_2H_4O), which have high emissivity in the atmospheric window, can also be used for radiative cooling.[9,10] These results well demonstrate the capabilities of radiative cooling technology. However, the primary cooling power is usually required during the day.

For passive daytime radiative cooling (PDRC), high emissivity in the atmospheric window and high reflectivity in the solar spectrum are required. There are some studies on radiative cooling coatings.[11–17] For example, Huang and Ruan[15] proposed a method of achieving daytime radiative cooling through a double-layer coating, composed of top layer and bottom layer of acrylic resin infused with TiO_2 and carbon black particles, respectively. The coating can theoretically achieve more than 90% solar reflection and an average emissivity of more than 0.9 in the sky window. Peoples *et al.*[16] used TiO_2 particles of various sizes in nanocomposites to enhance solar reflectance, the results show that the selected combination of particle size and concentration can broaden the spectral scattering peak. Its radiative cooling coating could have high spectral reflectance in the solar spectrum but a lower emissivity in the atmospheric window spectrum. Researches of photonic crystals and metamaterials with radiative properties[18–24] provide new ideas for daytime radiative cooling. Raman *et al.*[21] designed a planar photonic device structure, composed of seven alternating layers of hafnium oxide (HfO_2) and SiO_2. The structure can be cooled by about 4.9 °C, below ambient temperature during the day. The three thick layers on the top

†Corresponding author. E-mail: yongminzhou@njtech.edu.cn

© 2023 Chinese Physical Society and IOP Publishing Ltd

mainly affect the infrared emissivity, covering the wavelength range of 8 μm–13 μm. And the four thinner bottom layers act as a one-dimensional photonic crystal, with a maximum solar reflection of 97%. Hossain *et al.*[22] demonstrated experimentally that anisotropic metamaterials can be tuned to have strong and strictly selective infrared emission, with a nearperfect overlap of 8 μm–13 μm. It was estimated that the projected cooling power exceeds 100 $W \cdot m^{-2}$ and a cooling potential is 12 °C lower than the ambient temperature. In addition to the above studies, other researches of radiative cooling have also been conducted, such as the cooling of solar cells,[25,26] decorative attractive color protective paints,[27] and windshields for maintaining cooling performance.[28]

Among the existing passive daytime radiative cooling materials, metamaterials and photonic crystal materials have excellent radiation cooling performance. However, they often require complex and expensive processing equipment, which cannot be massproduced, especially the application of energy saving in buildings has tremendous obstacles. To solve this problem, it is necessary to produce radiative cooling coatings with better radiative cooling performance that can be used on a large scale for building insulated applications.

Meanwhile, in most of the double-layer coating structures in which TiO_2 particles are used to reflect solar radiation, a single material is chosen for designing the emissive layer so as to achieve the radiative properties and increase the emissivity of the coatings in the atmospheric window by increasing the thickness. In practical applications, the thicker coating has disadvantages such as small usage range, high cost, and easy to crack. Therefore, in this work, we choose two inorganic materials, SiO_2 and Si_3N_4 particles, to be added to the resin matrix to achieve a low-thick double-layer coating structure that can achieve a daytime radiative cooling effect through the synergistic effect of the materials. We first use the finite-difference time-domain (FDTD) algorithm to optimize particle size and film thickness in the infrared band.[29] The hybrid particles are deposited on the Al surface. Their reflectivity and emissivity are characterized. Then wed investigate the cooling power. Finally, the effect of conduction and convection on the cooling power are studied.

2. Simulation and preparation

We design a two-layer coating structure with micron particles (see Fig. 1). It comprises a top layer for reflecting solar radiation and a bottom layer with emissive properties in the atmospheric transparent window. The influence of factors, such as particle size and thickness of the material, on the emissive performance will be studied in the following subsection.

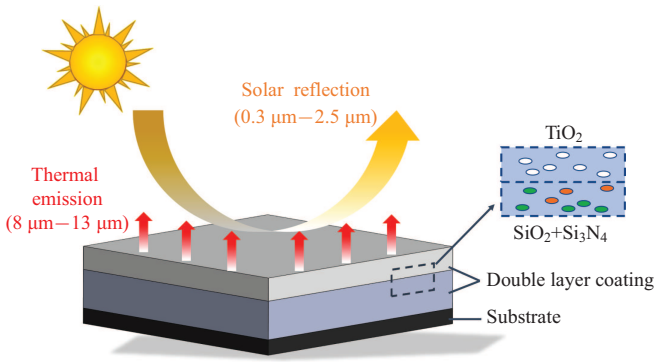


Fig. 1. Schematic diagram of two-layer radiative cooling coating with mixture of particles.

2.1. Materials selection

In the study of the radiative cooling coatings, the thermoplastic acrylic resin is chosen as the base material because of its high transparency, excellent weather resistance, and ability to form a film at room temperature and dry quickly. Two materials, SiO_2 and Si_3N_4, are chosen for the emitter layer. Figure 2 shows that SiO_2 and Si_3N_4 have high k-values (extinction coefficients) in their corresponding wavelength regions of the atmospheric window,[30] and the high k-values indicate the rapid attenuation of electromagnetic waves that are eventually absorbed by the material. The SiO_2 film has high k values in a wavelength range of 810 μm, and the Si_3N_4 film has high k values in a broader region above 6 μm. In the high-k area, each material exhibits high emissivity, which is caused by strong phonon polarization resonances. Mixing materials and superimposing their optical properties make it possible to achieve high emission properties throughout the sky window.

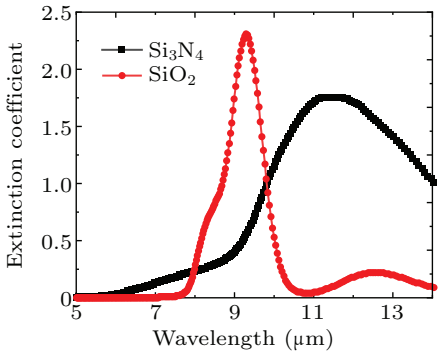


Fig. 2. Curves of extinction coefficient value (k) *versus* wavelength of SiO_2 and Si_3N_4 thin films.

Submicron TiO_2 particles (anatase and rutile) have been shown to scatter sunlight strongly and act as effective solar reflectors.[31] Therefore, we use a particle radius of 0.5 μm and a volume fraction of 10% to achieve the effect of solar reflection, which have been extensively studied.[14,15] There will be no need to mention them here particularly later.

2.2. Model building

The numerical FDTD solutions software is an optical simulation and analysis software based on the FDTD algorithm for

solving Maxwell's equations in three dimensions, which has a wide range of applications in the design, analysis, and optimization of optical materials and photonic devices. A periodic structure of a specific size represents the simulation domain of a coating composed of particles. Because the volume fraction of particles is too large, it is not conducive to cast, film formation, and poor light transmission. The particle volume fraction is chosen to be 10% in the simulation. The refractive index parameters of SiO_2 and Si_3N_4 arecited from Ref. [32].

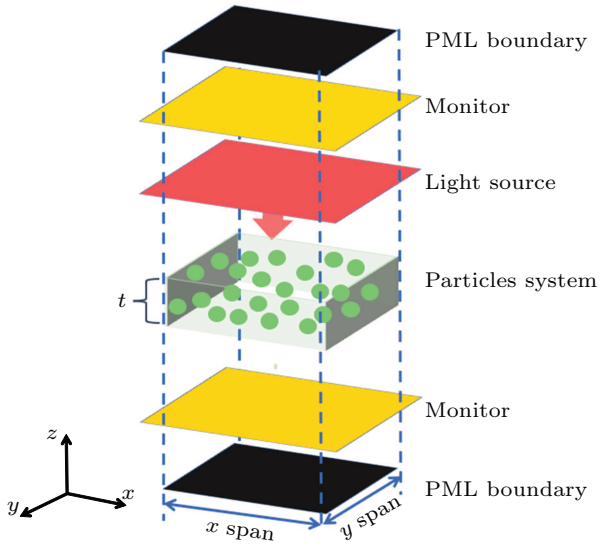


Fig. 3. Simulation domain of FDTD simulation.

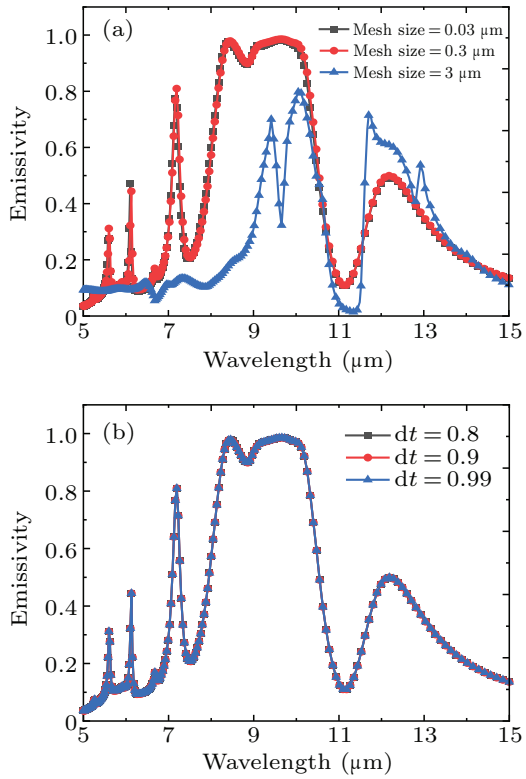


Fig. 4. Curves of predicted emissivity of SiO_2 coatings *versus* wavelength for different values of (a) grid size and (b) dt stability factor.

After fitting the material parameters, setting the geometric modeling and calculation area. The schematic diagram of the simulation domain can be obtained as shown in Fig. 3. The x span and y span are both 10 μm, and the thickness is in a range of 5 μm–25 μm. While the x direction and the y direction are both set to be periodic, the z direction is set to be in a non-periodic condition. The mesh accuracy meets the calculation requirements. Figure 4 shows the effect of the grid size and dt stability factor on the emissivity. When the SiO_2 is coated with 1.5-μm-radius particles and the coating thickness reaches 5 μm, it can seen that convergent results can be achieved by using a mesh size of 0.03 μm. The mesh step size of 0.03 μm is chosen for the subsequent calculation. At the same time, the dt stability coefficient has little influence on the simulation results within the considered range. Considering the calculation cost, the dt stability coefficient is selected as 0.9 for calculation. Taking the light source as plane wave, its spreading area in the x direction should be larger than the calculation area, and its propagation should be in the negative direction of the z direction. Then the reflectivity monitor is positioned above the incident light and the transmittance monitor is placed underneath the coating. It is worth noting that the attention must be paid to selecting an appropriate distance between the monitor and the boundary.

2.3. Optimization of particle size and coating thickness

The effect of SiO_2 particle size on the performance of radiative cooling coating is first investigated. To study the size effect of the particles, we first set the thickness to 25 μm. When the size parameter ($x = 2\pi r/\lambda$) is approximately equal to 1, the Mie resonance peak appears.[14] In this work, the radii of SiO_2 particles are selected to be 1 μm, 1.5 μm, and 2 μm, respectively. The simulation results of the predicted emissivity in a range of 5 μm–15 μm are shown in Figs. 5(a)–5(c). Figure 5(d) shows the comparison of predicted emissivity among SiO_2 coatings with particle radii in a range of 8 μm–13 μm. It can be observed that the curves of predicted emissivity *versus* wavelength of the coatings have similar trends in the wavelength range between 8 μm and 10.5 μm. And the particles with radius of 1.5 μm have the highest emissivity in the wavelength region between 11.5 μm and 13 μm. Therefore, the particle radius is set to 1.5 μm in the following studies.

Based on the above simulation results, the average emissivity of SiO_2 coatings with different particle radii in a range of 8 μm–13 μm is calculated (see Fig. 6). It can be seen from the figure that the average emissivity of disordered particles increases with the increase in particle size. The average emissivity of the coating at $r = 1.5$ μm does not differ much from that at $r = 2$ μm. The average coating emissivity is greater than 0.8 when the particle radius is 1.5 μm. Still, the overall coating average emissivity does not reach 0.9, owing to the low coating emissivity in the particle radius range of 10.5 μm–11.5 μm.

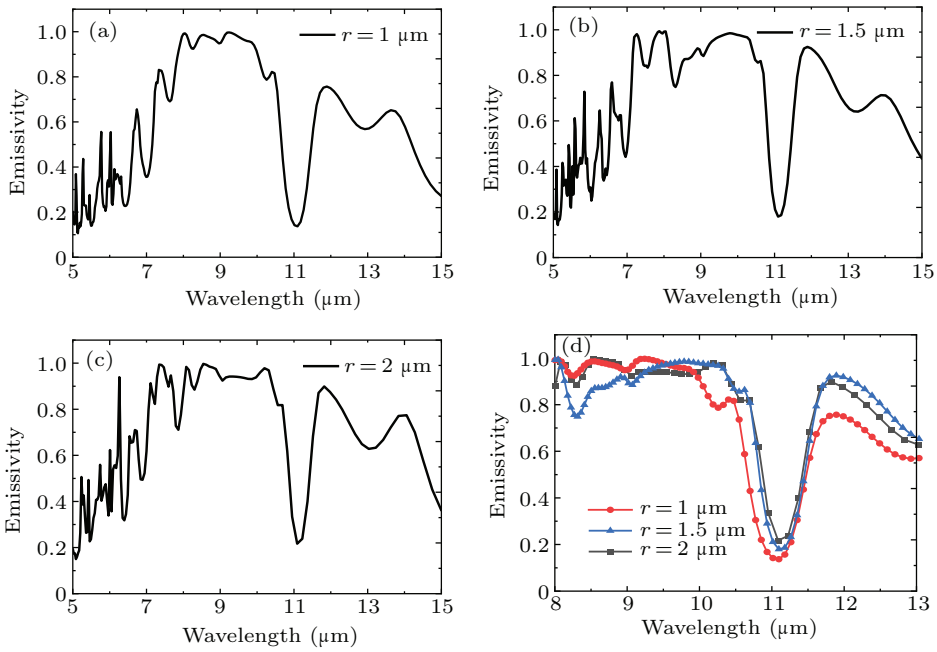


Fig. 5. Curves of predicted emissivity *versus* wavelength of SiO_2 coatings with radius 1 μm (a), 1.5 μm (b), 2 μm (c) at $t = 2.5$ μm. (d) Comparison of predicted emissivity among SiO_2 coatings with particle radii in a range of 8 μm–13 μm.

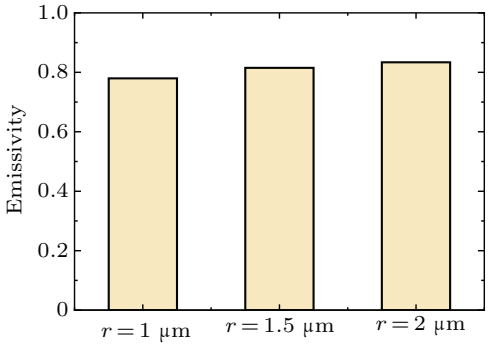


Fig. 6. Average emissivity of coatings in particle radius range of 8 μm–13 μm.

The effect of thickness of densely packed particles on the coating emissivity is further investigated. And the simulation results of the predicted emissivity in the range of 5 μm–15 μm are shown in Figs. 7(a)–7(c). Figure 7(d) shows a comparison of predicted emissivity among the SiO_2 coatings with different thicknesses in the range of 8 μm–13 μm. The trends of IR emissivity varying with wavelength for different thickness are almost identical. As the coating thickness increases, the emissivity in the 11.5 μm–13 μm band increases. When the thickness is 5 μm, the emissivity is low, around 0.4. However, when the thickness is above 25 μm, the emissivity of the coating is sufficiently high.

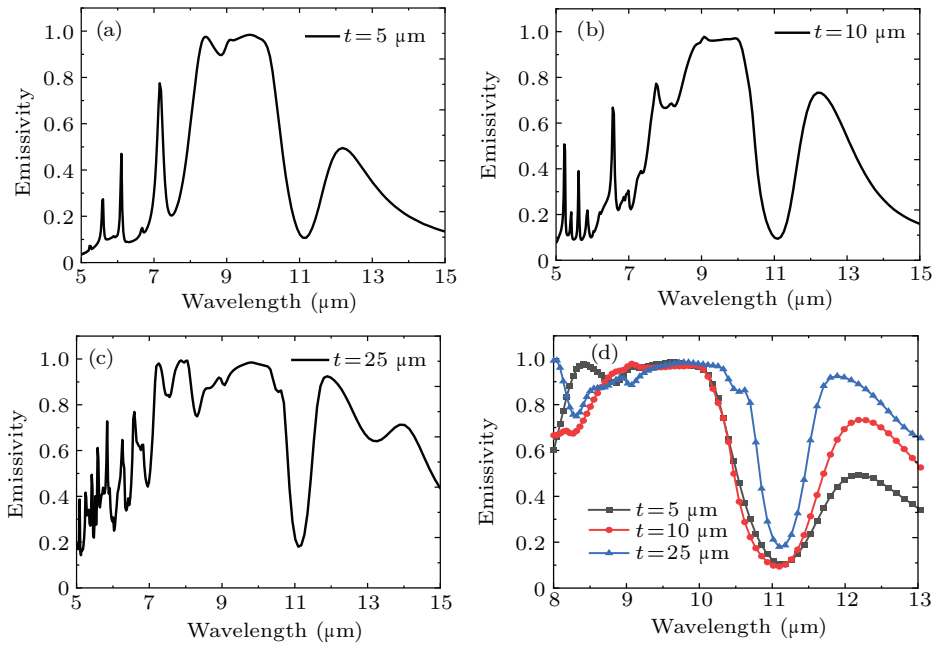


Fig. 7. Curves of predicted emissivity of SiO_2 coating *versus* wavelength for thickness $t = 5$ μm (a), 10 μm (b), and 25 μm (c) at $t = 1.5$ μm. (d) Comparison of predicted emissivity among SiO_2 coatings *versus* wavelength with thicknesses in a range of 8 μm–13 μm.

The average emissivity of SiO_2 coatings with different thicknesses in the range of 8 μm–13 μm is shown in Fig. 8. With the increase in thickness, the average emissivity of the disordered particle system shows an increasing trend. When the film thickness is 5 μm, the average IR emissivity at 8 μm–13 μm is only 0.67. However, when the film thickness increases to 25 μm, the average IR emissivity rises to 0.82.

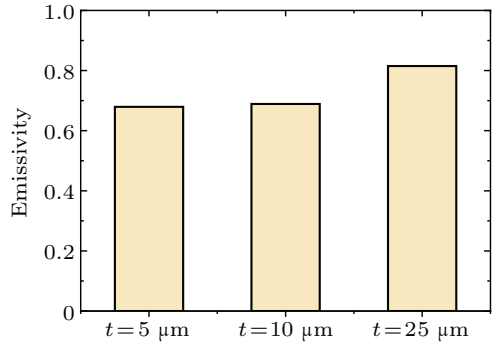


Fig. 8. Average emissivity of coatings in the range of 8 μm–13 μm at different coating thicknesses.

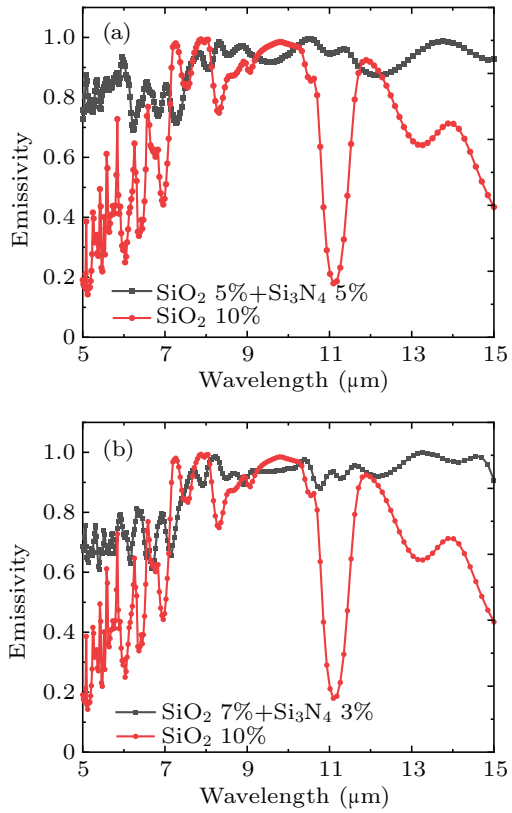


Fig. 9. Curves of predicted emissivity *versus* wavelength of mixed coatings with mixing ratio of 1:1 (a) and 7:3 (b) at $t = 25$ μm and $r = 1.5$ μm.

At the same time, comparing the influence of coating particle radius and thickness on emissivity, the emissivity is generally lower in the range of 10.5 μm–12 μm. To improve the overall emissivity of the coating, the optimal particle radius and coating thickness of the SiO_2 coating simulation are retained, then a model with $t = 25$ μm and $r = 1.5$ μm is selected to study the effect of the addition of SiO_2 and Si_3N_4 particles. The effect of dopant content on the coating emissivity is investigated. The existing 1.5 μm-radius Si_3N_4 particles are irregularly shaped, and to facilitate the study of their effect on the radiative properties of the coatings, spherical particles are adopted here.

The predicted emissivity values of mixed coatings with different mixing ratios of SiO_2 particles to Si_3N_4 particles are shown in Fig. 9. It can be found that a highly selective emissivity within the transparency atmospheric window can be achieved owing to the synergy of the optical properties of the material. The addition of Si_3N_4 particles is beneficial to the improvement of the emissivity of the radiation coating in the wavelength region between 10.5 μm and 12 μm. And the average emissivity of the mixed coatings added in two mixing ratios is over 0.9 in the range of 8 μm–13 μm.

2.4. Fabrication

Based on the results of theoretical simulations, the rutile TiO_2 (1 μm), SiO_2 (3 μm), and Si_3N_4 (3 μm) particles are selected to prepare coatings for the experiments. Figure 10 provides the particle size distributions and morphological characterizations of raw material. The results show that the SiO_2 and TiO_2 particles are relatively regular spherical particles with smooth surfaces, while the Si_3N_4 particles are irregularly shaped.

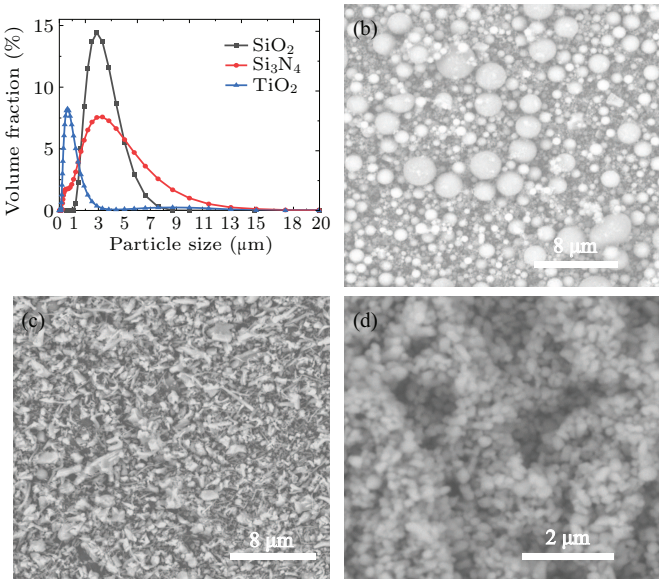


Fig. 10. (a) Particle size distributions. (b) SEM image of SiO_2 particles. (c) SEM image of Si_3N_4 particles. (d) SEM image of TiO_2 particles.

In the first step of the coating preparation, the acrylic resin is mixed with N, N-dimethylformamide (DMF) solvent to prepare the solution. The volume ratio between solute and solvent is about 1:3. The solution is then stirred with a magnetic stirrer for 30 min until the solute is completely dissolved and SiO_2 and Si_3N_4 microparticles with different ratios are added. Then the solution is stirred for 1 h to obtain uniform suspensions,

during which an anti-settling and leveling agent are added to improve the coating performance. The prepared dispersion solution is dropped onto the Al substrate, and the mixed coatings embedded with SiO_2 and Si_3N_4 microparticles are applied using a wire rod applicator by controlling the rotational speed. Then the deposited film layer is dried at room temperature for 1 h. To prepare a two-layer coating, a second layer of the dispersion solution is placed at the top in the same way and dried at room temperature. To ease fabrication, a hybrid coating with a thickness of 120 μm is prepared here by scratch coating. The photograph of the double-layer coatings painted on an Al substrate, surface, and cross-sectional SEM images for coating prepared by 1:1 ratio are shown in Fig. 11. The total thickness of the double layer coating is about 179 μm.

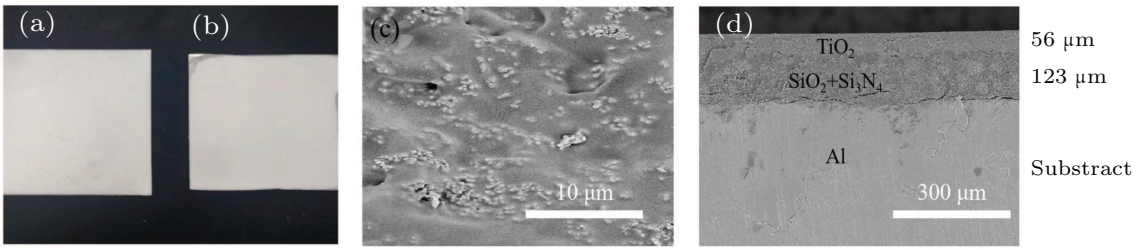


Fig. .11 (a) Photo of coating with 7:3 ratio, (b) photo of the coating with 1:1 ratio, (c) SEM image of the coating from the top view, and (d) cross-sectional view SEM image.

3. Results and discussion

3.1. Radiation properties of coatings

The reflectance of the coatings in the solar spectral region (0.3 μm–2.5 μm) is measured by using a UV–Vis–NIR spectrophotometer (UV-3600i Plus, Shimadzu, Japan) and an integrating sphere. Specular reflectance in a wavelength band of 2.5 μm–15 μm is measured by using a Fourier transform infrared spectrometer (Nicolet IS-50, Thermal Sciences). Because the measured coating is opaque, the absorptivity of the coating can be calculated by $A = 1 - R$. In the formula, A is the spectral absorptance, R is the reflectance. And the emissivity of the coating can be further obtained according to Kirchhoff's thermal radiation law.[14]

The measured spectral emissivity values of 120-μm-thick hybrid coatings with different mixing ratios on Al substrates are shown in Fig. 12(a). Layers mixed with SiO_2 and Si_3N_4 have high reflectivity in the solar radiation region (0.3 μm–2.5 μm) and high emissivity in the infrared area (2.5 μm–15 μm). The high reflectivity values of the two coatings in the wavelength band of 0.3 μm–2.5 μm are mainly due to the strong scattering effect of the TiO_2 particles, and gradually disappear with the increase of the wavelength. While the mixture coating with a 1:1 ratio on the Al substrate has higher emissivity in the wavelength band of 0.3 μm–2.5 μm due to the relatively low band gap energy of Si_3N_4 and the increase in its content, which affects solar reflection.[28] The spectral emissivity of the double-layer coating depends mainly on the underlying emissive layer. Owing to the superposition of the high-k region of SiO_2 and Si_3N_4, high emissivity is achieved for the entire atmospheric transparency window, which is consistent with the theoretical simulation result. The emissivity spectra of the two double-layers are similar, and the hybrid coating with a 1:1 ratio added has better emission performance in the wavelength range of 8 μm–13 μm. This may be because Si_3N_4 films have high k values in the wavelength range above 6 μm. An increase in Si_3N_4 content, caused by strong phonon-polarization resonance effects increases the emissivity of the coating. The reflectance of the coating prepared at a 1:1 ratio exceeds 0.9 at 0.4 μm–1.6 μm, and the average reflectance in the solar spectrum reaches 87.6%. The average emissivity of 2.5 μm–15 μm is 92%.

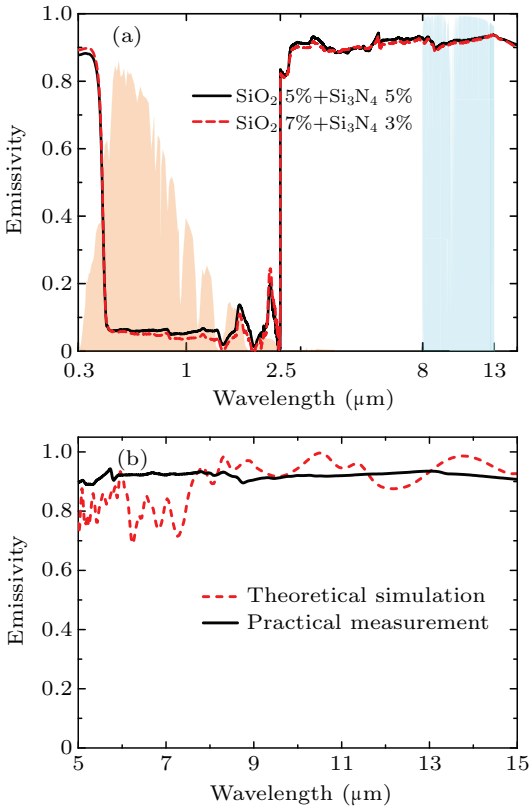


Fig. 12. (a) Curves of measured emissivity of mixed coatings with different mixing ratios. (b) Comparison of simulated coating emissivity with measured coating emissivity in a range of 5 μm–15 μm.

The comparison between simulated emissivity and measured emissivity of the 120-μm-thick radiative cooling coating

prepared at 1:1 addition in a wavelength range of 5 μm–15 μm is shown in Fig. 12(b). The results show that the average emissivity of the coatings in the range of 5 μm–8 μm increases from 0.82 to 0.92 as the thickness increases. And the simulation results fluctuate within a specific range compared with the measured emissivity in the 8 μm–15 μm band, which may be attributed to the fact that the simulations are performed with a certain accuracy and that the raw material may also have errors due to incomplete dissolution during the actual sample preparation.

3.2. Theoretical cooling performance

When the radiative cooling material is exposed to a clear sky, it will spontaneously radiate heat outward radiation, but also absorbs thermal radiation from the sun, atmospheric thermal radiation, and its non-radiative heat transfer. Assuming that the ambient temperature is $T_{\rm amb}$ and the surface temperature of the radiative cooling material is T, the cooling power per unit surface area $P_{\rm cool}(T)$ can be expressed as[33]

$$P_{\rm cool}(T) = P_{\rm rad}(T) - P_{\rm atm}(T_{\rm amb}) - P_{\rm sun} - P_{\rm nonrad}, \quad (1)$$

where $P_{\rm rad}$ is the power emitted from the surface of the radiative cooling materials, $P_{\rm atm}$ is the power absorbed from the atmospheric projected radiation, $P_{\rm sun}$ is the power absorbed by solar thermal radiation, and $P_{\rm nonrad}$ is the absorbed power due to heat conduction and convection, all in units of $\rm W{\cdot}m^{-2}$. It can be calculated from the following equation:[16]

$$P_{\rm rad}(T) = \int_0^{\infty} \varepsilon(\lambda) E_{\rm b\lambda}(T,\lambda) {\rm d}\lambda, \quad (2)$$

$$P_{\rm atm}(T_{\rm amb}) = 2\pi \int_0^{\pi/2} \int_0^{\infty} \varepsilon(\lambda) \varepsilon_{\rm atm}(\lambda,\theta) \times E_{\rm b}(T_{\rm amb},\lambda) {\rm d}\lambda \cos\theta {\rm d}\theta, \quad (3)$$

$$P_{\rm sun} = \int_0^{\infty} \varepsilon(\lambda) E_{\rm AM1.5}(\lambda) {\rm d}\lambda, \quad (4)$$

$$P_{\rm nonrad} = h_{\rm c}(T_{\rm amb} - T), \quad (5)$$

where $E_{\rm b\lambda}(T,\lambda)$ is the monochromatic emissive power of the surface at temperature T and wavelength λ, $\varepsilon(\lambda)$ denotes the spectral emissivity of the coating at wavelength λ. $\varepsilon_{\rm atm}(\lambda,\theta)$ represents the atmospheric emissivity, and its value is $\varepsilon_{\rm atm}(\lambda,\theta) = 1 - t(\lambda,0)^{1/\cos\theta}$, $t(\lambda,0)$ refers to the atmospheric transmittance in the zenith direction, $E_{\rm AM1.5}(\lambda)$ is the solar radiance, and the integral over a range of 0.3 μm–2.5 μm is about 900 $\rm W{\cdot}m^{-2}$, and $h_{\rm c}$ is the non-radiative heat transfer coefficient.

From the viewpoint of emissivity, passive radiative coolers can be divided into selective emitter and broadband emitter. Their difference lies in the fact that the broadband emitter has an infrared emissivity of 1 in all but for the range of 0.3 μm–2.5 μm. For the broadband emitter, when the temperature of the radiative cooler is lower than the atmospheric temperature, the power absorbed from the atmosphere increases, which is not conducive to achieving radiative cooling. When the surface temperature is higher than a certain value, 280 K, which is cited from Ref. [15], the increase in emission is better than the increase in absorption, and the broadband emitter has a better cooling capacity.[15,34,35] In practical applications, the building surface temperature is higher than the atmospheric temperature under direct daytime sunlight conditions. The material temperature for radiative cooling over the building surface is usually set to be higher than the atmospheric temperature.

To analyze the radiative cooling performance of our bilayer hybrid coating, we perform theoretical calculations at different values of surface temperature T. First, we assum that the ambient temperature is 300 K. Second, the heat convection caused by temperature difference and the energy transfer triggered off by heat conduction cannot be ignored. Generally, the non-radiative heat transfer coefficient ranges from 0 to 12 $\rm W{\cdot}m^{-2}{\cdot}K^{-1}$. Here, $h_{\rm c} = 4$ $\rm W{\cdot}m^{-2}{\cdot}K^{-1}$ is selected in cooling power calculation. At the same time, it is compared with the cooling power without non-radiative heat transfer. The calculated relationship between cooling power and the temperature difference is shown in Fig. 13.

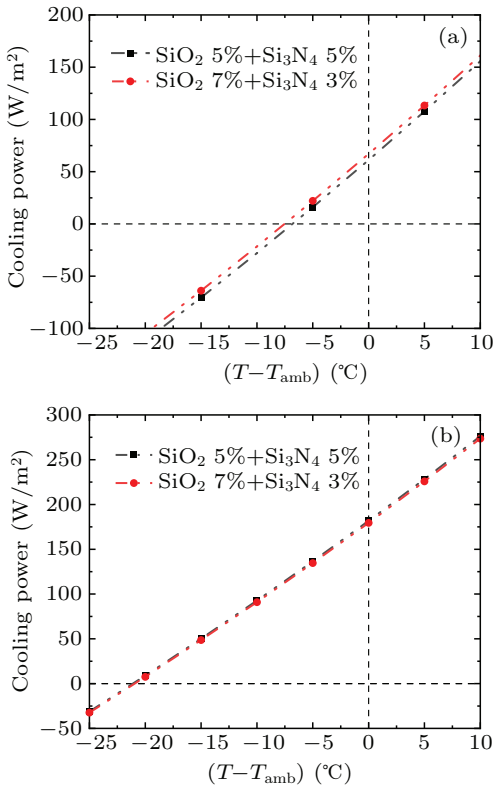


Fig. 13. Theoretical cooling power under different temperature differences (a) at daytime and (b) at nighttime.

Figure 13(a) shows the radiative cooling power at different temperature differences of coatings during the day. Under direct sunlight (AM1.5), a hybrid coating with a 7:3 ratio addition of SiO_2 and Si_3N_4 can theoretically achieve a cooling power of 67 $\rm W{\cdot}m^{-2}$ when the surface temperature is

the same as the ambient temperature. And the hybrid coating with a 1:1 ratio addition can achieve a cooling power of 61 $W{\cdot}m^{-2}$. Both layers can theoretically achieve a cooling capacity of about 8 °C below the ambient temperature (when $h_c = 4\ W{\cdot}m^{-2}{\cdot}K^{-1}$). Furthermore, if the non-radiative heat transfer is neglected, the hybrid coating with 7:3 addition can theoretically achieve about 15 °C below the ambient temperature.

Figure 13(b) shows the radiative cooling performances of the coatings during the night at different surface temperatures. When the surface temperature is the same as the ambient temperature, the hybrid coating added at a 1:1 ratio addition has a larger cooling power (about 180 $W{\cdot}m^{-2}$), and both coatings achieve similar stagnation temperatures, which are theoretically about 21 °C below the ambient temperature (when $h_c = 4\ W{\cdot}m^{-2}{\cdot}K^{-1}$). In addition, if non-radiative heat transfer is neglected, the mixed coatings with different ratios all can reach approximately 40 °C below the ambient temperature.

The cooling performance of the coatings are further investigated by considering conduction and convection heat exchange. We consider three different values of non-radiative heat transfer coefficient h_c of 0, 6 $W{\cdot}m^{-2}{\cdot}K^{-1}$, and 12 $W{\cdot}m^{-2}{\cdot}K^{-1}$, in which h_c = 6 $W{\cdot}m^{-2}{\cdot}K^{-1}$ and 12 $W{\cdot}m^{-2}{\cdot}K^{-1}$ denote wind speeds of 1 m/s and 3 m/s, respectively.[36] Figure 14 shows the relationships between cooling power and surface temperature of the hybrid coating added with a ratio of 1:1 at different non-radiative heat transfer coefficients.

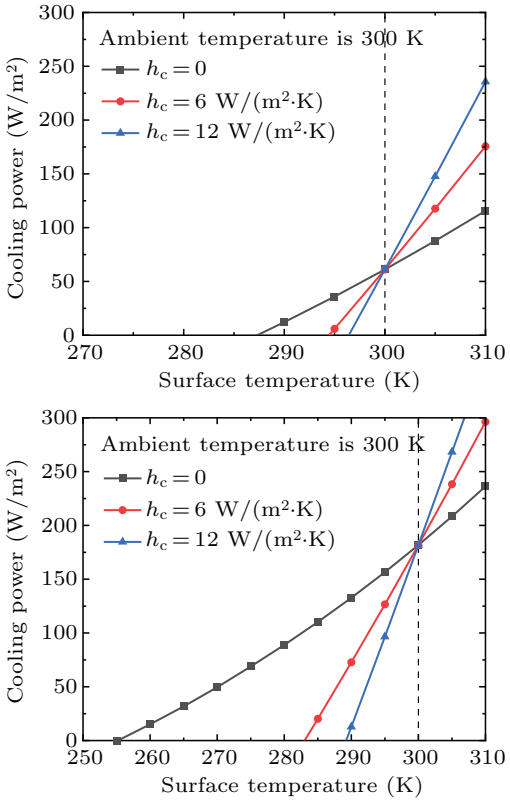


Fig. 14. Relationship between temperature difference and theoretical cooling power at different values of h_c at (a) daytime and (b) nighttime.

As shown in Fig. 14, the coating has the same cooling power for different non-radiative heat transfer coefficients when the coating surface temperature is the same as the ambient temperature. Owing to the neglect of solar thermal radiation at night, the corresponding radiative cooling flux increases. When the surface temperature of the coating is higher than the ambient temperature, the net radiative cooling flux of the composite coating keeps increasing because the temperature difference causes the coating to dissipate heat to the outside. When the surface temperature of the coating is lower than the ambient temperature, the net radiative cooling flux of the coating becomes smaller and smaller because the temperature difference causes the coating to absorb external heat. When the value of the radiative cooling flux decreases to 0, the surface temperature of the coating reaches its minimum value. During the daytime, the minimum surface temperatures of the coating are 287 K ($h_c = 0$), 294.5 K ($h_c = 6\ W{\cdot}m^{-2}{\cdot}K^{-1}$), and 296 K ($h_c$ = 12 $W{\cdot}m^{-2}{\cdot}K^{-1}$) for different non-radiative heat transfer coefficients, respectively.

3.3. Experimental results of cooling performance

To obtain the actual cooling effect of coatings, a 120-μm-thick hybrid coating with a particle size of 3 μm is prepared. And a volume fraction of both SiO_2 and Si_3N_4 of 5% is selected here for the radiative cooling experiments on the roof in Nanjing, the uncoated Al film and the ambient temperature are also selected as the control experimental factors. The experimental setup and its internal schematic are shown in Fig. 15. Polystyrene foam box is used for isolating the heat exchange between the coating and the outside environment. A PE film is used on the top to ensure that the energy emitted by the layer can enter into outer space while reducing the air convection effect. Wood needles support the coating to prevent the floor for heating. And for daytime radiative cooling experiments, the surface is covered with aluminum foil to reduce solar radiation. The temperature of the inner surface of the coating is measured by using a thermocouple, while the ambient temperature is calculated by using a device with no PDRC coating placed on it.[37]

We conducte daytime outdoor experiments from 10:00 a.m. to 15:30 on April 15, 2023 when the humidity was 38%. The test results are shown in Fig. 16(a). The results show that the temperature of the double-layer radiative cooling coating is always lower than the ambient temperature under direct sunlight, reaching an average of 5 °C below the ambient temperature and about 12 °C below the temperature of the Al film. Although the aluminum film can reflect part of the sunlight, the temperature of the aluminum film is about 7 °C higher than the ambient temperature. It is important to note that our temperature measurement points are located inside the PE film-sealed cavity, which produces a greenhouse effect dur-

ing daytime measurements.[37] Hence, the temperature inside the box is higher than the outdoor atmospheric temperature. Also, weather conditions (wind speed, humidity, and cloudiness) significantly affect outdoor test results.[34] The increase in cloud cover during daytime measurements can lead to significant fluctuations in test temperature.

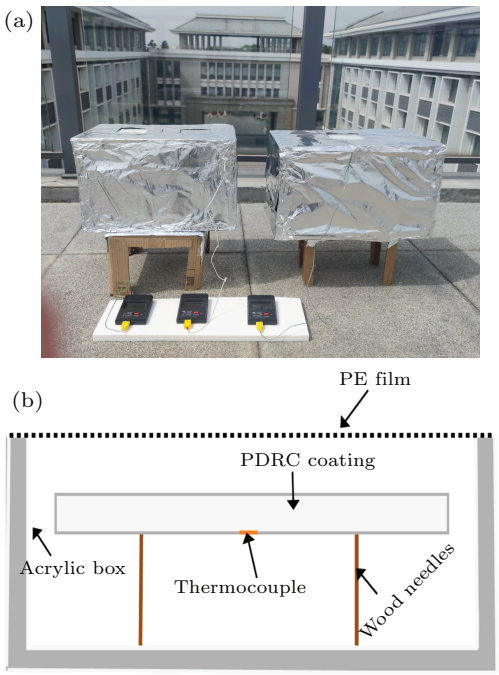


Fig. 15. (a) Photos of outdoor experimental setup and (b) diagram of inner part of the device.

The night cooling experiment was measured from 19:00 to 22:00, with an average wind speed of 1.4 m/s and humidity of 52%. The test results are shown in Fig. 16(b). As can be seen from the figure, both the Al film temperature and the ambient temperature measured inside the sealed cavity of the PE film are lower than the ambient air temperature measured outside the device at night. The double radiative cooling coating has no cooling effect compared with the ambient temperature measured inside the sealed PE film cavity, indicating that the broadband radiative cooler is more suitable for environments where the temperature is higher than the atmospheric temperature. However, its temperature can be about 1.6 °C below the temperature of the Al film, and it can be cooled by about 4 °C compared to the ambient air temperature measured outside the experimental setup.

Our prepared coatings are compared with other coatings in order to evaluate the cooling performance of our coatings. A comparison of our coating is made with a double-layer radiative cooling coating ($\varepsilon = 0.90$) containing TiO_2 particles and SiO_2 particles cited from Ref. [14], showing that the hybrid coating with a 1:1 ratio addition of SiO_2 and Si_3N_4 can increase the average emissivity of the "atmospheric window" spectrum by 2.2%. And it is beneficial to the theoretical cooling of 3 °C during the day when $h = 4$ W·m^{-2}·K^{-1}. Another comparison of our coating is conducted with the single-layer radiative cooling coating ($\varepsilon = 0.86$) cited from Ref. [17], indicating that adding a 1:1 ratio of hybrid coating can increase the average emissivity of the "atmospheric window" spectrum by 6.9%.

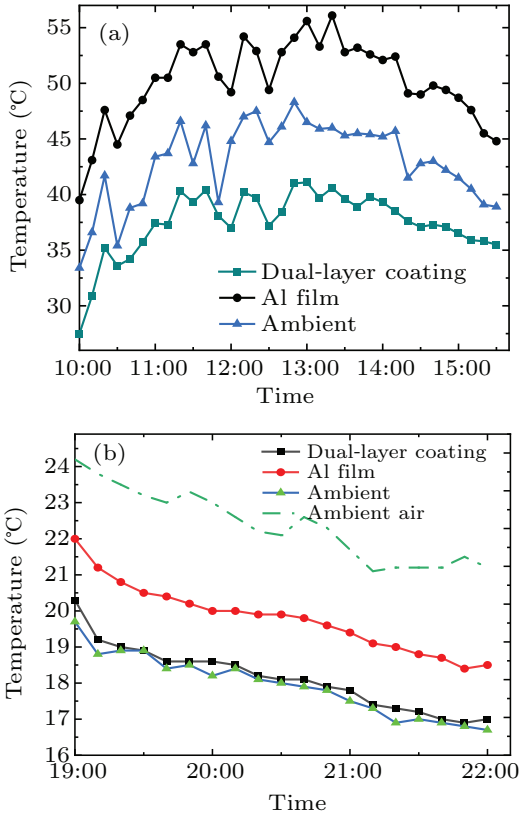


Fig. 16. Experimental results during (a) daytime and (b) nighttime.

4. Conclusions

In summary, a cost-effective double-layer coating embedded with TiO_2, SiO_2, and Si_3N_4 micro particles in acrylic resin, which can improve cooling performance, are proposed in this work. The simulation results show that the particle size of 3 μm can give the best cooling performance and the coating thickness should be above 25 μm for SiO_2 coating. Meanwhile, the addition of Si_3N_4 particles is beneficial to the improvement of the emissivity of the radiation coating. The coatings prepared by mixing different ratios of SiO_2 to Si_3N_4 all have good PDRC optical properties. On an Al substrate, the overall reflectance of the mixed coating added with a ratio of 1:1 in the solar spectrum reaches 87.6% and the emittance is 92% in the atmospheric transparency window. Under dry air condition and assuming non-radiative heat transfer coefficient $h_c = 4$ W·m^{-2}·K^{-1}, the cooling power values of these coatings are calculated with the measured spectral emissivity. Both coatings can be theoretically cooled by about 8 °C during the daytime and about 21 °C at nighttime. The achieved equilibrium temperature is lower than the ambient temperature, indicating that even after considering the significant conduction

and convective heat exchange, the cooling effect still exists. Daytime outdoor experiments show that the radiative cooling coating temperature is lower than the ambient temperature and that the coating has a cooling effect.

References

[1] Guo C L, Liu C, Jiao S K, Wang R S and Rao Z H 2020 *Appl. Therm. Eng.* **173** 115207
[2] Zhou Y K, Zheng S Q and Zhang G Q 2020 *Energy* **192** 116608
[3] Bhatia B, Leroy A, Shen Y, Zhao L, Gianello M, Li D, Gu T, Hu J, Soljačić M and Wang E N 2018 *Nat. Commun.* **9** 5001
[4] Mandal J, Fu Y, Overvig A C, Jia M, Sun K, Shi N N, Zhou H, Xiao X, Yu N and Yang Y 2018 *Science* **362** 315
[5] Miyazaki H, Okada K, Jinno K and Ota T 2016 *J. Ceram. Soc. Jpn.* **124** 1185
[6] Granqvist C G and Hjortsberg A 1981 *J. Appl. Phys.* **52** 4205
[7] Gentle A R and Smith G B 2010 *Nano Lett.* **10** 373
[8] Miyazaki H, Yoshida S, Sato Y, Suzuki H and Ota T 2013 *J. Ceram. Soc. Jpn.* **121** 242
[9] Lushiku E M, Hjortsberg A and Granqvist C G 1982 *J. Appl. Phys.* **53** 5526
[10] Lushiku E M and Granqvist C G 1984 *Appl. Opt.* **23** 1835
[11] Harrison A W and Walton M R 1978 *Sol. Energy* **20** 185
[12] NilssonI T M J, Niklasson G A and Granqvist C G 1992 *Sol. Energ. Mater. Sol. Cells* **28** 175
[13] Nilsson T M J and Niklasson G A 1995 *Sol. Energ. Mater. Sol. Cells* **37** 93
[14] Bao H, Yan C, Wang B X, Fang X, Zhao C Y and Ruan X L 2017 *Sol. Energ. Mater. Sol. Cells* **168** 78
[15] Huang Z F and Ruan X L 2017 *Int. J. Heat Mass Transfer* **104** 890
[16] Peoples J, Li X Y, Lv Y B, Qiu J, Huang Z F and Ruan X L 2019 *Int. J. Heat Mass Transfer* **131** 487
[17] Xu Z, Li N, Liu D, Huang X, Wang J, Wu W, Zhang H, Liu H, Zhang Z and Zhong M 2018 *Sol. Energ. Mater. Sol. Cells* **185** 536
[18] Diatezua D M, Thiry P A, Dereux A and Caudano R 1996 *Sol. Energ. Mater. Sol. Cells* **40** 253
[19] Zhu L, Raman A and Fan S 2013 *Appl. Phys. Lett.* **103** 223902
[20] Zhu L X, Raman A, Wang K X, Anoma M A and Fan S H 2014 *Optica* **1** 32
[21] Raman A P, Anoma M A, Zhu L, Rephaeli E and Fan S 2014 *Nature* **515** 540
[22] Hossain M M, Jia B H and Gu M 2015 *Adv. Opt. Mater.* **3** 1047
[23] Wu J Y, Gong Y Z, Huang P R, Ma G J and Dai Q F 2017 *Chin. Phys. B* **26** 104201
[24] Huang J G, Xuan Y M and Li Q 2014 *Chin. Phys. Lett.* **31** 094207
[25] Tang H J, Zhou Z H, Jiao S F, Zhang Y F, Li S, Zhang D B, Zhang J, Liu J W and Zhao D L 2022 *Sol. Energ. Mater. Sol. Cells* **235** 111498
[26] Gentle A R and Smith G B 2016 *Sol. Energ. Mater. Sol. Cells* **150** 39
[27] Smith G B, Gentle A, Swift P, Earp A and Mronga N 2003 *Sol. Energ. Mater. Sol. Cells* **79** 163
[28] Bathgate S N and Bosi S G 2011 *Sol. Energ. Mater. Sol. Cells* **95** 2778
[29] Dyachenko P N, Do Rosário J J, Leib E W, Petrov A Y, Kubrin R, Schneider G A, Weller H, Vossmeyer T and Eich M 2014 *ACS Photon.* **1** 1127
[30] Chae D, Lim H, So S, Son S, Ju S, Kim W, Rho J and Lee H 2021 *ACS Appl. Mater. Inter.* **13** 21119
[31] Vargas W E 2000 *J. Appl. Phys.* **88** 4079
[32] Palik E D 1985 *Handbook of Optical Conctants of Solids* (San Diego: Academic Press) pp. 719–772
[33] Yao H W, Wang X X, Yin H Y, Jia Y L, Gao Y, Wang J Q and Fan C Z 2021 *Chin. Phys. B* **30** 064214
[34] Meng S, Long L S, Wu Z X, Denisuk N, Yang Y, Wang L P, Cao F and Zhu Y G 2020 *Sol. Energ. Mater. Sol. Cells* **208** 110393
[35] Song X H, Gao Y F and Zhang P 2022 *J. Mater. Chem. A* **10** 22166
[36] Duffie J A and Beckman W A 2013 *Solar Engineering of Thermal Processes*, fourth edn. (New Jersey: John Wiley & Sons Inc) p. 164
[37] Zhang Y L and Yu J 2021 *ACS Appl. Nano Mater.* **4** 11260